Post-print of: Wachowski S., Kamecki B., Winiarz P., Dzierzgowski K., Mielewczyk-Gryń A., Gazda M.: Tailoring structural properties of lanthanum orthoniobates through an isovalent substitution on the Nb-site. Inorganic Chemistry Frontiers. Iss. 9 (2018), pp. 2157-2166. DOI: 10.1039/C8QI00524A

Tailoring structural properties of lanthanum orthoniobates through an isovalent substitution on Nb-site

Sebastian Wachowski*[1], Bartosz Kamecki[1], Piotr Winiarz[1], Kacper Dzierzgowski[1], Aleksandra Mielewczyk–Gryń[1] and Maria Gazda[1]

[1] Department of Solid State Physics, Faculty of Applied Physics and Mathematics, Gdańsk University of Technology, Narutowicza 11/12, 80-233 Gdańsk, Poland

*corresponding author: sebastian.wachowski@pg.edu.pl, tel.+48 58 348 66 12, address: Centrum Nanotechnologii A, ul. Narutowicza 11/12, 80-233 Gdańsk

Keywords:

lanthanum orthoniobate, lanthanum orthoarsenate, proton conductors, fergusonite, scheelite, monazite, thermal expansion, isovalent substitution

Abstract

Tetragonal polymorph of lanthanum orthoniobate can be stabilized to room temperature by the substitution of Nb with an isovalent element. $LaNb_{1-x}As_xO_4$ ($0 < x \leq 0.3$), where As is an element stabilizing tetragonal structure, were successfully synthesized with combined co-precipitation and solid-state reaction method. The phase transition temperature, above which the material has tetragonal structure, decreases linearly with increasing As-content, and $LaNb_{0.7}As_{0.3}O_4$ is tetragonal at room temperature. The analysis of the influence of different isovalent substituents, namely V, Sb and Ta, has shown that there is a relation between the properties of the chemical element and its effect on the structure. It was proposed that the electronegativity of the substituent determines the type of stabilization – the tetragonal/monoclinic structure is stabilized by chemical elements with electronegativity higher/lower than that of niobium. The slope of the phase transition temperature dependence on the substituent content has been proposed as a parameter determining the "quality" of the stabilization, since steeper function leads to a larger decrease of transition temperature for the same content of different substituents. The analysis has shown that the stabilization of tetragonal structure, apart from the electronegativity, depends also on ionic radius of a substituent. Arsenic has been found to be a better stabilizer of the tetragonal polymorph of lanthanum orthoniobate than Sb, but worse than V.

1. Introduction

Ion conducting ceramics have gained a growing interest around the globe as functional materials for electrochemical devices, like batteries [1], gas sensors [2,3], fuel cells [2–6], electrolysers [3,7], gas membranes [3,8] or reaction chambers [9,10]. A material with properties such as chemical stability and high-temperature tolerance, combined with high ionic conductivity defines a nearly perfect candidate for a component of these devices.

High-Temperature Proton Conductors (HTPCs) are ceramics, typically ternary oxides [11–15], which at elevated temperatures conduct hydrogen ions - protons. HTPCs do not contain hydrogen in their composition, therefore hydrogen ion is regarded as a structural defect, so-called protonic defect, which is transported via Grotthuss mechanism [14,15].

In the group of proton conducting oxides, doped lanthanum orthoniobates have been gathering scientific interest in the last two decades [12,16–27]. Lanthanum niobate, when acceptor doped on La-site, is a proton conductor in a wide range of temperatures (400-1000 °C) and oxygen partial pressures (from 2.5 % wet O_2 to 2.5 % wet H_2) [12,19,25,26]. The highest protonic conductivity of 10^{-3} S/cm at 800 °C was achieved for 1 mol% Ca-doped $LaNbO_4$ [12], however several other attempts with different acceptor dopants (such as Ba [26], Sr [25,26] and Mg [19]) were done and lead to similar results.

Lanthanum orthoniobate has two polymorphs: low-temperature monoclinic fergusonite (space group no. 15, I2/c) [28] and high-temperature tetragonal scheelite (space group no. 88, $I4_1/a$) [29]. The phase transition between them is of second order and occurs, in undoped material, at roughly 500 °C [30–33]. The change of the crystal structure affects many properties, which can raise challenges for future applications. Especially two of materials' properties are essential in that respect. First, thermal expansion coefficient (TEC) changes nearly twofold with the transition [18,24]. Changes in the TEC can yield thermal incompatibility between different components which may lead to strain, cracking, delamination and even failure of the device. Another factor that changes with the structure is the apparent activation energy E_A of the protonic transport, which is lower for the tetragonal polymorph of $LaNbO_4$ [19,22,34]. While La-site doping is typically done in order to change electrical properties since the impact on the structural properties is limited [26,35–37], however the studies have shown that doping on the Nb-site affects the phase transition temperature [17,20,22,24,27,38–40]. Therefore there is a possible solution to avoid the effects induced by the phase transition. An appropriate substitution can lower the phase transition temperature T_p below room temperature (RT) making the structure of the material tetragonal from RT up to 1000 °C [20,24]. This is the case in lanthanum orthoniobates with vanadium [20,24,38] or antimony [24] substitutions. Another way is to substitute

niobium with tantalum, which causes the opposite effect, i.e. it stabilizes the monoclinic structure and shifts the phase transition into higher temperature range [17,24,27]. Another element, which could potentially be used as an isovalent substituent is arsenic. From the chemical point of view this element belongs to the same group as antimony, therefore a similar influence on the structural properties could be expected. The substitution should also affect the electrical properties since it was shown that Sb-substituted $LaNbO_4$ is a proton conductor, which exhibits higher conductivity than undoped lanthanum orthoniobate [22]. Moreover, lanthanum arsenate - $LaAsO_4$ – is also a proton conductor, with a protonic conductivity of ~10^{-5} S/cm at 800 °C in wet oxidizing conditions.

This work aim includes two essential parts: (I) it presents results of structural and thermomechanical studies of lanthanum niobate substituted on the niobium site with arsenic and (II) provide extensive comparative analysis of the influence of substitution of Nb with different isovalent elements from the 5th and 15th group of the periodic table.

2. Experimental

$La_1Nb_{1-x}As_xO_4$, where x = {0.05;0.1;0.15;0.2;0.25;0.3;}, samples were synthesized with a two-step route. In the first step $LaAsO_4$ and $LaNbO_4$ were synthesized. $LaAsO_4$ was obtained from $La(NO_3)_3x6H_2O$ (Chempur, Germany, 99.99%) and As_2O_5 (Alfa Aesar, Germany, 99.9%) aqueous solutions by a co-precipitation method described elsewhere [41]. $LaNbO_4$ was synthesized via the solid-state reaction route starting from La_2O_3 (Alfa–Aesar, Germany, 99.99% preheated at 900°C) and Nb_2O_5 (Alfa Aesar, Germany, 99.99%). The samples were calcined at 1200 °C for 8 hours. The second step was a solid-state reaction of $LaAsO_4$ and $LaNbO_4$ according to equation (1):

$$xLaAsO_4 + (1-x)LaNbO_4 \rightarrow LaNb_{1-x}As_xO_4 \quad (1)$$

The powders were first mixed in the stoichiometric amounts and ball milled in isopropanol for 12 h in a Fritsch Pulverisette 7 planetary ball mill using zirconia balls and cups. The slurry obtained from milling was dried at 100 °C for 5 h and pressed into pellets under pressure of 100 MPa. In the last step, in which the reaction (1) occurred, the green bodies were heated in air at 1200 °C for 8h and then at 1400 °C for 8h.

Powder X-ray diffraction analysis was performed using the Phillips X'Pert Pro MPD with $CuK_{\alpha1}$ and $CuK_{\alpha2}$ radiation. In order to determine unit cell parameters, XRD patterns were analysed with Rietveld refinement method using the FullProf Suite software[42]. As an initial

point of the analysis, unit cell parameters of the fergusonite (space group no. 15, I2/c) [28] and scheelite (space group no. 88, $I4_1/a$) [29] crystal structures of $LaNbO_4$ were utilized. For $LaAsO_4$ a monazite (space group no. 14, $P2_1/n$) [43] crystal structure was used. In the case of precursor materials only LeBail fit was used, whilst on final compositions Rietveld refinement was performed with the Thomson Cox Hastings profile function.

The relative length change of the sintered samples was measured by Netzsch DIL 402 PC/4 dilatometer in argon at the temperature range 50 – 1000°C with heating/cooling rate of 2°C/min. The density of the bulk samples was determined by the Archimedes method.

Micrographs of the pellets were obtained using FEI Quanta FEG 250 Scanning Electron Microscope with Everhart-Thorney detector in a high vacuum mode. Based on the micrographs, average grain size was calculated with the average grain intercept method. In each micrograph at least 15 random straight lines were drawn to determine the grain size. Averaged values from all lines were used for the average grain size of the current sample and a standard deviation was calculated as an uncertainty.

3. Results

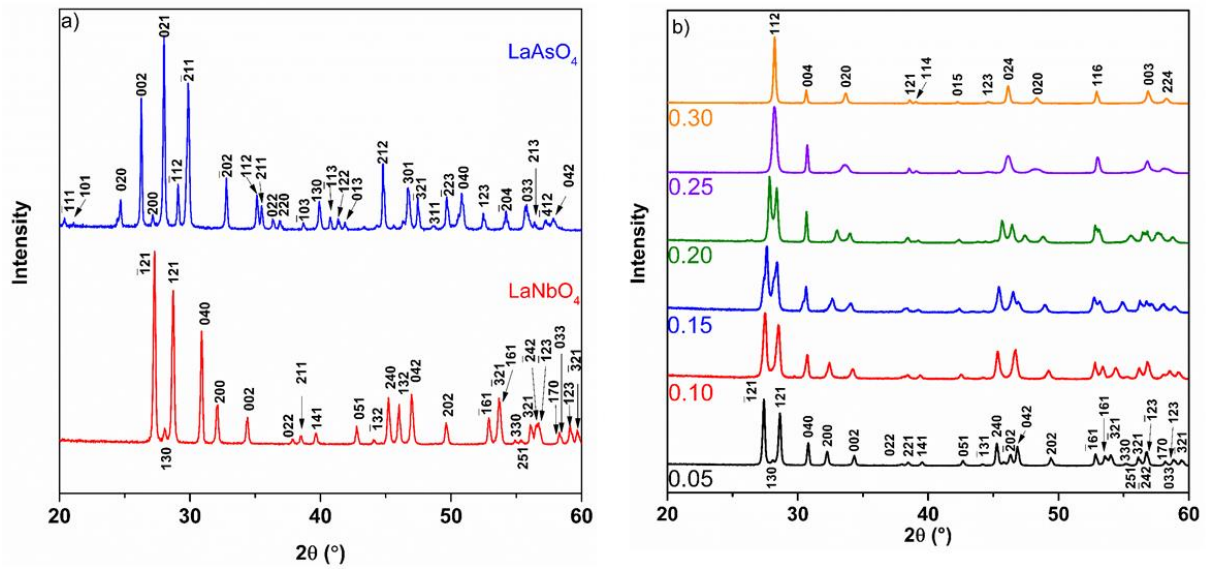

Figure 1. X-ray diffractograms of a) the precursor materials and b) $LaNb_{1-x}As_xO_4$ with different As content.

The precursors, $LaAsO_4$ and $LaNbO_4$, used in the second step of synthesis have been checked by XRD to confirm that expected phases were formed and no impurities were present. The results are shown in Figure 1.a. In the diffractogram of $LaAsO_4$ all the reflections are indexed with monazite structure, whereas in that of $LaNbO_4$ - with monoclinic fergusonite structure.

The diffractograms have been refined with the LeBail method and the determined unit cell parameters are summarized in Table 1. At room temperature, both $LaAsO_4$ and $LaNbO_4$ have monoclinic structures described with the $P2_1/n$ and I2/c space groups, respectively.

Table 1. Unit cell parameters of precursor materials determined by LeBail fit

Compound	**Space group**	**a (Å)**	**b (Å)**	**c (Å)**	**β (°)**	**V (Å^3)**
$LaNbO_4$	I2/c	5.5656	11.5215	5.2029	94.08	332.79
$LaAsO_4$	$P2_1/n$	6.7879	7.2110	7.0072	104.67	331.79

The X-ray diffractograms of $LaNb_{1-x}As_xO_4$ are shown in Figure 1.b. In the diffractograms of the samples with As content below 20 mol%, all reflections are indexed within the low-temperature monoclinic polymorph of $LaNbO_4$, whilst the material substituted with 30 mol% of As has tetragonal scheelite structure at room temperature. In the case of $LaNb_{0.75}As_{0.25}O_4$, the reflections belong to the tetragonal structure but their shape indicate also the presence of the monoclinic phase with not-well resolved XRD reflections.

To visualize the structural changes occurring in the materials unit cells of monoclinic and tetragonal $LaNbO_4$ polymorphs have been drawn in Vesta software [44]. The unit cells are presented in Figure 2 along with the simple graphic presentation of the unit cells parallelepipeds and the relation between axes in different structures. The parameter along a unique axis in the monoclinic cell, b_m, corresponds to c_t in the tetragonal one. The base of the monoclinic unit cell is a parallelogram with sides, a_m and c_m, with different lengths and monoclinic angle β_m between them. In the tetragonal symmetry the base is a square with sides of a_t and the angle between them, equal to 90°, is denoted accordingly to crystallographic standards, namely γ_t.

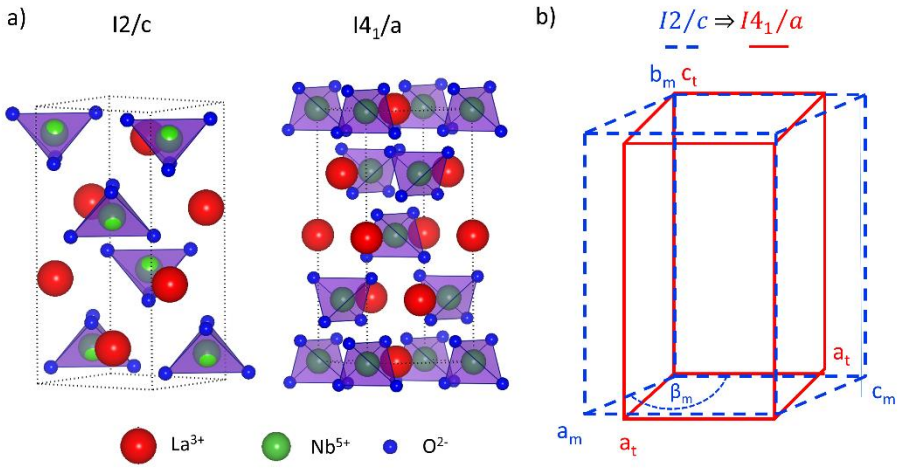

Figure 2. The unit cells of: a) monoclinic (space group I2/c) and tetragonal ($I4_1/a$) polymorphs of $LaNbO_4$ prepared with Vesta software [45] and b) a sketch showing relations between the unit cell parameters in the two structures.

Rietveld analysis allowed to determine the unit cell parameters which are presented as a function of As content in Figure 3. The R_{wp} factors of refinement were lower than 20 %. The R_{wp} factors along with the unit cell volumes and other structural and microstructural parameters are gathered in Table 2. First of all, the analysis confirmed that in the case of $LaNb_{0.75}As_{0.25}O_4$ the material is actually a dual-phase system consisting of the monoclinic and tetragonal polymorphs. The approximate contents of the monoclinic and tetragonal phases were, respectively, 65 and 35 vol%. All other samples were single phase as was also indicated by the initial analysis. The unit cell basal parameters as a function of As content are presented in Figure 3 a. As it can be seen a_m decreases, whereas c_m increases with As content. In the case of $LaNb_{0.7}As_{0.3}O_4$, the structure is tetragonal at room temperature, therefore, there is only one basal parameter a_t to which the a_m and c_m parameters converge with increasing As content. The monoclinic angle, as depicted in Figure 3 b, decreases monotonically towards 90 ° with the As content. Since the major difference between the fergusonite and scheelite structures is the basal plane of the unit cell, these changes show how the unit cell of $LaNb_{1-x}As_xO_4$ deviates from the monoclinic towards the tetragonal structure while As content is increased. The b_m parameter in the monoclinic structure, corresponding to c_t in the tetragonal one, increases with the arsenic content.

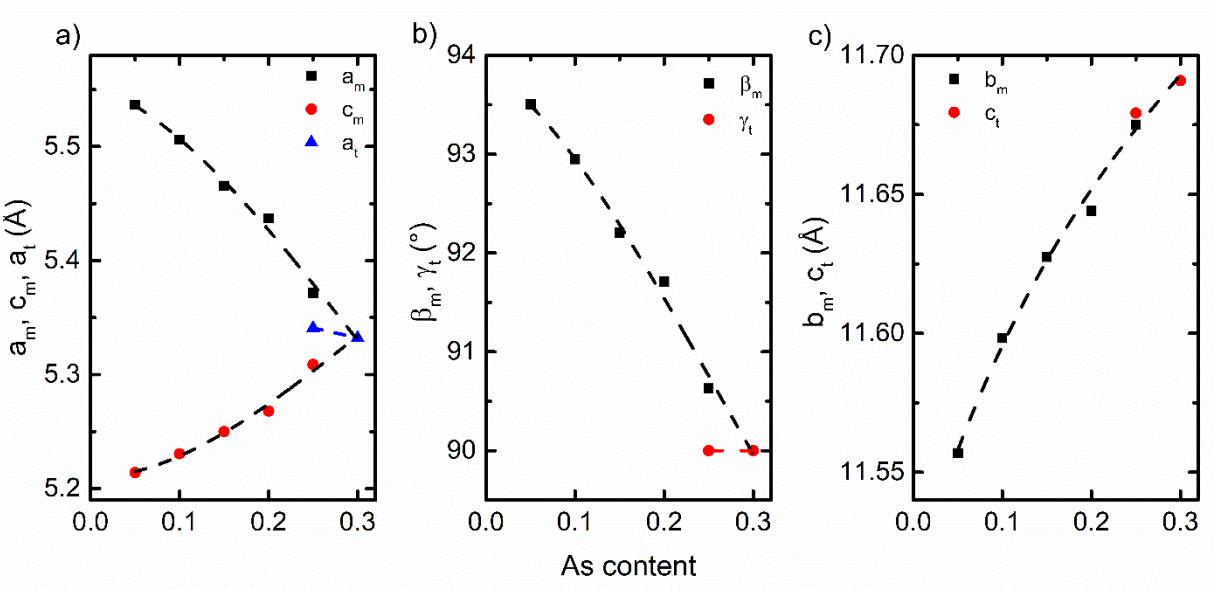

Figure 3. Unit cell parameters determined by Rietveld analysis. Subscripts m,t denote monoclinic and tetragonal phase respectively. a) unit cell basal parameters, b) angles c) b_m or c_t parameters. Dashed lines are to guide the eye only.

Table 2. *Structural parameters of $LaNb_{1-x}As_xO_4$, where x = 0.05 to 0.30. V denote unit cell volume, d_{AVG} – average grain size, R_{wp} – weighted profile factor of Rietveld refinement, ρ_m – measured density, ρ_t – theoretical density, ρ_{rel} – relative density*

As content	V (Å^3)	d_{AVG} (µm)	R_{wp} (%)	ρ_m (g/cm^3)	ρ_t (g/cm^3)	ρ_{rel} (%)
0.05	333.0(1)	4.9(3)	18	5.9(2)	5.838	99(2)
0.10	333.8(1)	2.7(2)	17	5.3(1)	5.823	90(2)
0.15	333.4(1)	2.4(2)	19	5.7(1)	5.810	98(2)
0.20	333.4(1)	2.1(2)	18	5.6(1)	5.804	96(2)
0.25					5.880	
(mono.)	332.9(2)	2.3(2)	17	5.6(2)	5.857	96(5)
(tetra.)	333.2(1)				5.838	
0.30	332.4(1)	2.6(3)	18	5.7(2)	5.821	99(2)

The SEM micrographs of the bulk sample surfaces are shown in Figure 4. The microstructure of all studied samples is similar. The samples are well-sintered ceramics with a good connection between the grains and, in some cases, a few small isolated pores and cracks propagating across

the crystal grains may be seen. The density measurements (*cf.* Table 2) have shown that the relative density is always above 90 % and in most of the cases above 95%.

The grain size and shape does not vary much between the micrographs and the values of the average grain sizes calculated with the average grain intercept method (presented in Table 2) are for most of the samples between 2.1 and 2.7 μm. The only exception is a sample containing 5 mol% of As in which case the size is 4.9 μm.

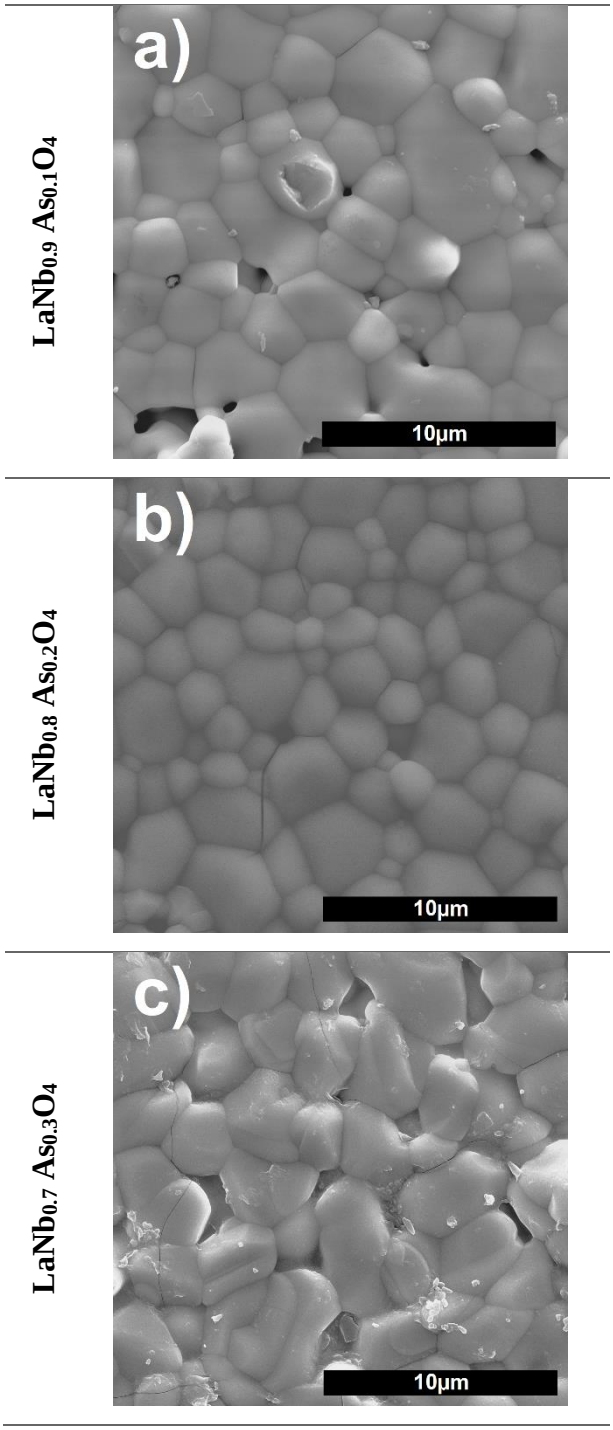

Figure 4. Scanning electron micrographs of the surface of a) $LaNb_{0.9}As_{0.1}O_4$, b) $LaNb_{0.8}As_{0.2}O_4$ and c) $LaNb_{0.7}As_{0.3}O_4$.

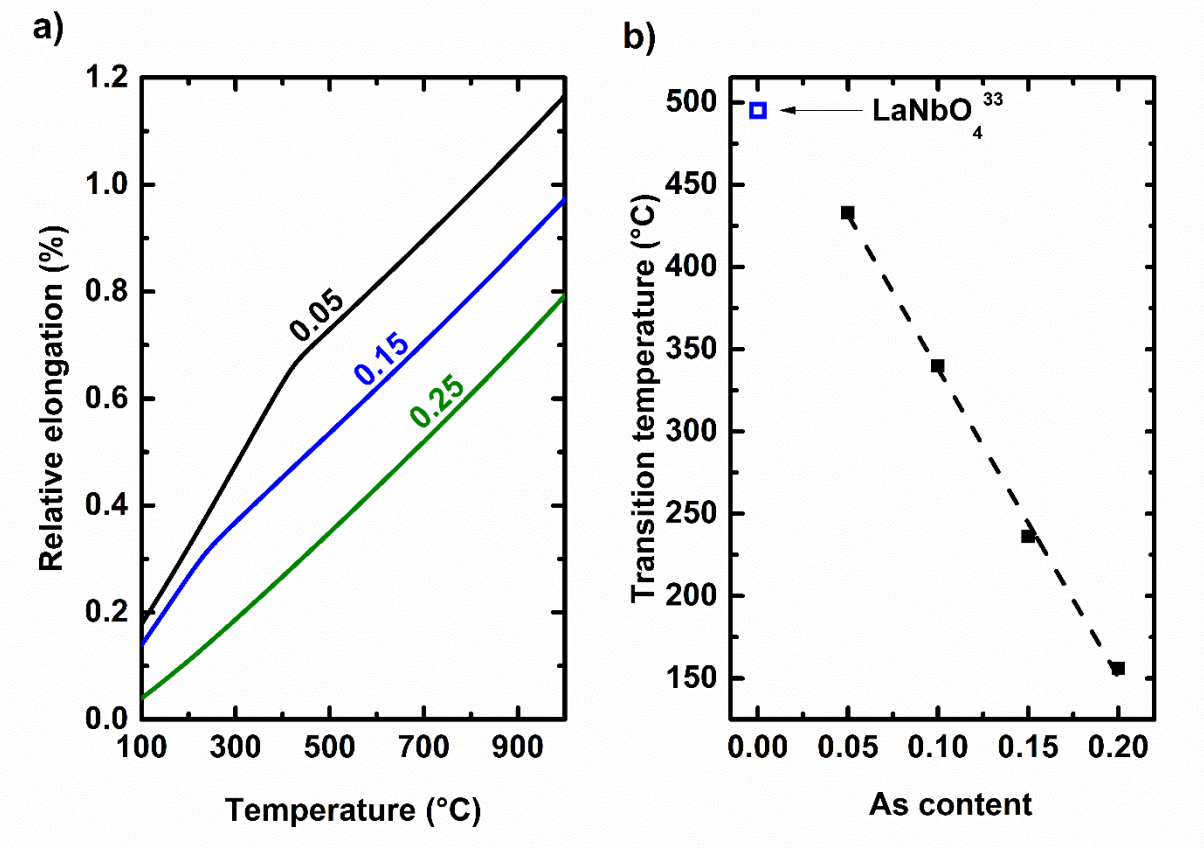

Figure 5. a) Relative elongation of $LaNb_{1-x}As_xO_4$ as a function of temperature, b) Temperature of phase transition versus As content (data for $LaNbO_4$ from ref. [33]).

The dense bulk specimens have been studied by the means of dilatometry. The relative elongation as a function of temperature for these materials is plotted in Figure 5 a). All the compositions containing up to 20 mol% of As showed two linear regions with a bend of the curve occurring between 100 and 450 °C depending on the composition. In the case of materials with 25 and 30 mol% As the relative elongation was a linear function of the temperature within the temperature range used in the measurement. Since in lanthanum orthoniobate system thermal expansion coefficient depends on the structure the temperature at which the coefficient changes can be used to determine the phase transition temperature. Determined in this way, transition temperature is plotted as a function of the As content in Figure 5 b. It is evident that the phase transition temperature is a linear function of the substituent content. $LaNb_{0.75}As_{0.25}O_4$, as showed by the Rietveld analysis, has a mixed monoclinic-tetragonal composition at room temperature and the dilatometric measurements indicate no phase transition between 100 and

1000 °C. Therefore, the full transformation to the tetragonal polymorph of lanthanum niobate must occur between room temperature and 100 °C. In the case of the material with 30 mol% As the structure is tetragonal, and no change of thermal expansion coefficient is observed, which indicates that material is tetragonal up to 1000 °C.

Table 2 Thermal expansion coefficients and transition temperatures of $LaNb_{1-x}As_xO_4$ samples.

As content	Thermal expansion coefficients (10^{-6} K^{-1})		Transition temperatures (°C)
	Monoclinic phase	**Tetragonal phase**	
0.05	15.0(1)	8.7(1)	433(6)
0.10	13.9(1)	8.6(2)	340(7)
0.15	12.6(2)	8.6(1)	236(6)
0.20	9.4(3)	8.2(2)	156(10)
0.25	-	8.4(1)	-
0.30	-	8.3(1)	-

Thermal expansion coefficients and phase transition temperatures are listed in Table 3. Whilst the coefficients for the tetragonal polymorph are similar and, in most cases, overlap within the uncertainty limit the values for the monoclinic phase are decreasing with increasing As content.

4. Discussion

Single phase materials have been obtained by the two-step method of synthesis (*cf.* Figure 1) for all compositions except $LaNb_{0.75}As_{0.25}O_4$. The existence of two different phases in the same thermodynamic conditions was observed previously[46] and can be explained by the means of two effects: 1) the temperature of the sample being close to a transition temperature and 2) a slightly different chemical composition of the samples' crystal grains. For the investigated system, the dilatometry results indicate that (cf. Figure 5, the phase transition for investigated samples must be below 100 °C) the first effect is present. Moreover, since the synthesis is basically a reaction between three or two different oxides and different diffusivity of elements yields different path lengths, some inhomogeneity should be expected.

From the microstructural point of view, the specimens present rather similar features. The porosity of the samples is generally decreasing with increasing As content. The only sample which stands out of this trend is $LaNb_{0.75}As_{0.25}O_4$. This sample, however, is a special case, because it is a two-phase system. First, the uncertainty of the determination of relative density

is increased due to the additional uncertainty of determination of phase fractions and phase duality may additionally change the sinterability of the material in an unforeseen way. Grain sizes are similar for almost all compositions. The only exception is the material with 5 mol% of As, in which grains are bigger. This cannot be explained without further experiments, which are beyond the scope of this study. However, one can argue that if the diffusivity of As is the lowest in the whole system then the material with the lowest concentration of the substituent may have the biggest grains.

It is interesting that the thermal expansion coefficients decrease with increasing concentration of the substituent, especially in the case of the monoclinic polymorph. This can be explained on the basis of the change of the bonds strength in the system induced by the substitution. Li et al. [47] argued that in ABO_4 oxides thermal expansion coefficient depends mostly on the A-O bond strength, thus if the concentration of the substituent increases the A-O bond strength then the thermal expansion coefficients should decrease. It has been shown that in the Sb-substituted lanthanum orthoniobates the Einstein temperature increases as the Sb content increases [48]. The increase is caused by stiffening of the optical vibration modes and, as it was argued by Mielewczyk-Gryń et al. [48], these relate to the vibrations between La^{3+} ions and BO_4^{3-} tetrahedra. Stiffening of vibration modes correlates with bond strength as stronger bonds will be stiffer. If the effect of As is similar to Sb then this also would explain the observed decrease of thermal expansion coefficient with increasing As concentration.

It has been shown that niobium substitution with 30 mol % of arsenic leads to the formation of a compound, which has tetragonal structure at room temperature (cf. Figure 1). As it was shown in Fig. 3, increasing As content causes the monoclinic angle decrease to 90°, whereas a_m and c_m converge to one value and b_m increases. This is a typical effect of a tetragonal phase stabilizer and has been observed previously for the other substituents [20,24]. Therefore, similarly to other pentavalent elements, namely V [20,24,38] and Sb [24], arsenic is a tetragonal phase stabilizer.

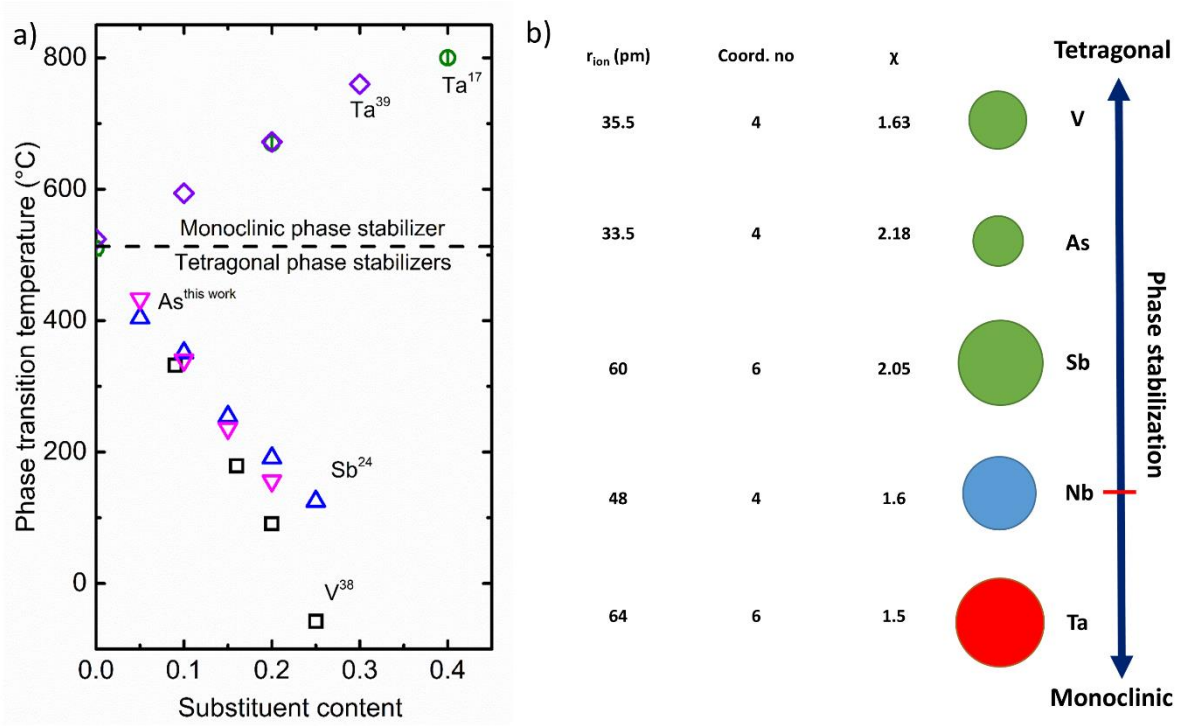

Figure 6. a) Relation between phase transition temperature and content of different Nb-site substituent (superscript indicates the reference) and b) diagram displaying ionic radius by Shannon (r_{ion}) [49], electronegativity (χ) and preferred coordination number of the substituent along with its influence on the phase stabilization properties (size of the circles and the ionic radius of the element are correlated).

In the following paragraphs, the effect of As-substitution on the structural properties of lanthanum orthoniobate will be discussed in comparison to the effects of other isovalent dopants, namely V [20,24,38], Ta [17,24,27,39] and Sb [24,35,48]. In order to better depict the influence of particular substituents, Fig. 6 presents the relations between the transition temperature and the content of a substituent (Fig. 6a) and qualitatively displays the roles of the elements along with their properties such as Shannon ionic radii [49], Pauling electronegativity, and coordination number (Fig. 6b).

The As, Sb and V elements are stabilizing the tetragonal phase, by decreasing the phase transition temperature. Tantalum has the opposite effect, meaning it shifts the transition temperature to higher temperatures. This also means that at selected temperature, with increasing Ta content the unit cell distorts more from tetragonal symmetry.

As presented in Fig. 5b the phase transition temperature in the As-substituted lanthanum orthoniobates depends linearly on the As content. In our previous work [24], we have found that a similar dependency is observed for Sb-substituted compounds. This kind of relations can be

also seen in Fig. 6, where the data obtained for all the discussed substituents is presented collectively. What makes particular elements different is the slope of the lines. In the case of As-, Sb- and V-doped materials it is $1.67(5)\times10^3$ K, $1.52(3)\times10^3$ K and $2.09(6)\times10^3$ K, respectively. We propose to use the value of the slope as a qualitative parameter classifying different substituents. The substituent that is characterized with the largest slope may be regarded as the best stabilizer of the tetragonal structure. This means that it requires the lowest substituent content for stabilization of the tetragonal phase at room temperature. The sample with the lowest content of substituent exhibiting tetragonal structure at room temperature is $LaNb_{0.75}V_{0.25}O_4$ [20,24], for materials containing As the exact content was not determined but it is between 0.25 and 0.30, whereas in Sb-substituted samples 0.3 is required to obtain a tetragonal specimen [24]. In that sense, the order from the best to worst tetragonal phase stabilizers would be V>As>Sb. Tantalum is the only example of the monoclinic phase stabilizer, therefore it can be simply inserted in this series of elements on the last position, thus V>As>Sb>Ta.

Figure 6 shows a set of properties of the substituents that could be potentially used to parametrize this relation. So far, a few explanations of how different types of substituents influence T_p have been proposed [17,20,24]. First, ionic radius of the substituent was proposed as the main factor [20]. This idea was based on the so-called Bastide diagram which relates room temperature structures of different ABO_4 compounds with r_A/r_O and r_B/r_O ionic radii ratios [50,51]. The diagram shows that all compound with the tetragonal structure at room temperature have lower r_B/r_O ratio than the monoclinic ones. Therefore, the introduction of a dopant smaller than Nb^{5+} leads to a decrease of T_p, whereas bigger ions would do the opposite. Another proposed factor was the preferred coordination number of the substituent ion in the parent structure [17]. In the tetragonal structure the B-site ion is 4-fold coordinated by the surrounding oxygen anions, whereas in the monoclinic structure the oxygen positions are distorted in such a way that the coordination of the B-site ion can be described as 4+2, where four oxygen sites are in the direct surrounding of the cation and two oxygen sites are a bit further away, yet still in its vicinity. Thus, intuitively 4-fold and 6-fold coordinated ions should respectively stabilize the tetragonal and monoclinic polymorphs of $LaNbO_4$. Both models explain well the properties of V- and Ta-doped materials, however, they do not explain the best-to-worst tetragonal stabilizers ordering, as As is the smallest ion, whilst the V is the best tetragonal stabilizer. Moreover, the effect of the Sb substitution completely falls out of this schema. As depicted in Figure 6 b antimony ion in $LaNbO_4$ in terms of ionic radius and coordination number is more similar to tantalum, rather

than vanadium, therefore it should stabilize the monoclinic phase. Meanwhile, it affects the material properties in the opposite manner.

In our previous work [24], where structural properties of V, Ta and Sb-doped lanthanum orthoniobates were studied, electronegativity and electron configuration has been analysed. It was shown that there is no correlation between the electron configuration and the phase transition, however, it seemed that electronegativity plays also an important role as it is related to covalent properties of the bonds and bond stiffness. Tsunekawa et al. [28] studied the properties of phase transition in pure lanthanum niobate and shown that the phase transition is correlated with the covalence of the B-O bond, which is the most shortened one during the transition. Moreover, it is important to understand that the more covalent bonds will have higher directionality, in contrast to 'pure' ionic bonds which are directionless. Thus, the effect would be that BO_4^{3-} tetrahedra become more rigid as a unit, due to a stronger covalent directional bond between B cation and O anion, whereas the interaction between the tetrahedra themselves, stemming from the ionic directionless bond, is weakened. This has been confirmed by the low-temperature heat capacity studies [48,52], which have shown that Debye temperature is decreasing with increasing vanadium or antimony content. The decrease of Debye temperature is related to softening of the inter-tetrahedron vibration modes, thus indicating softening of the bonding. It is important to note that tetrahedra must re-align while phase transformation occurs and as the interaction softens, the temperature high enough to allow re-alignment, is getting decreased. That is a reason why the electronegativity and phase transition temperature are linked. The link can be directly observed in Figure 6 b), where each element with electronegativity higher than Nb is a tetragonal phase stabilizer, whilst Ta with lower electronegativity stabilizes monoclinic polymorph. This link does not explain the ordering, however, it sets the ground rule. Therefore, the overall effect must be a superposition of more than one fundamental property of a substituent.

One may more precisely analyse the effect of different properties of the substituents by looking at how the phase transition of substituted samples deviates in relation to the parent structure as a function of varying effective properties of the B-site cations. Figure 7 displays the deviation of phase transition temperature δT_p as a function of either electronegativity $\delta\chi_{eff}$ or ionic radius $\delta r_{ion,eff}$ deviations. The phase transition temperature deviation is determined as follows:

$$\delta T_P = T_p - T_{p,0} \qquad (2)$$

where T_p is a phase transition temperature of a substituted sample and $T_{p,0} = 495$ °C [28] is a phase transition temperature of the non-substituted lanthanum niobate.

The deviation of the effective electronegativity is determined by the relation:

$$\delta\chi_{eff} = \chi_{eff} - \chi_{Nb} \quad (3)$$

where χ_{eff} is the effective electronegativity of the B-site element in the material with formula $LaNb_{1-x}M_xO_4$ (where M = V, Ta, As or Sb) and is given by the relation $\chi_{eff} = (1-x)\chi_{Nb} + x\chi_M$, where χ_{Nb} is the electronegativity of niobium and χ_M is the electronegativity of a substituent.

The effective B-site ionic radius deviation is given as:

$$\delta r_{ion,eff} = r_{ion,eff} - r_{Nb} \quad (4)$$

where $r_{ion,\,eff}$ is the effective ion radius on B-site in a sample of a general formula $LaNb_{1-x}M_xO_4$ (where M = V, Ta, As or Sb) and is given by the relation $r_{ion,eff} = (1-x)r_{Nb} + xr_M$, where r_{Nb} is the ionic radius of niobium and r_M is the ionic radius of a substituent.

Figure 7 shows that deviation of the phase transition temperature depends linearly on both deviations of ionic radius and electronegativity. According to the data to get lower phase transition temperature the electronegativity deviation must be positive (and opposite for the increase of T_p) it does not mean that higher deviation produces lower transition temperature. This is clearly seen in the case of the V-substituted samples where the deviation of electronegativity is very low, while the deviation of transition temperature is large and negative. The other tetragonal phase stabilizers, As and Sb, present high deviations of electronegativity, which are correlated with high deviations of transition temperature. On the negative side of electronegativity deviation data from Ta-substituted samples is presented and the effect of an increase of T_p is observed.

The linear type of relation is also observed when the deviation of the effective ionic radius is analysed (cf. Figure 7 b). The As- and V-substituted materials have increasingly lower values of δT_p as the deviation of the ionic radius becomes more negative. This tendency is also consistent with the behaviour of Ta doped samples, whereas the opposite type of relation is observed in the case of Sb-containing specimens.

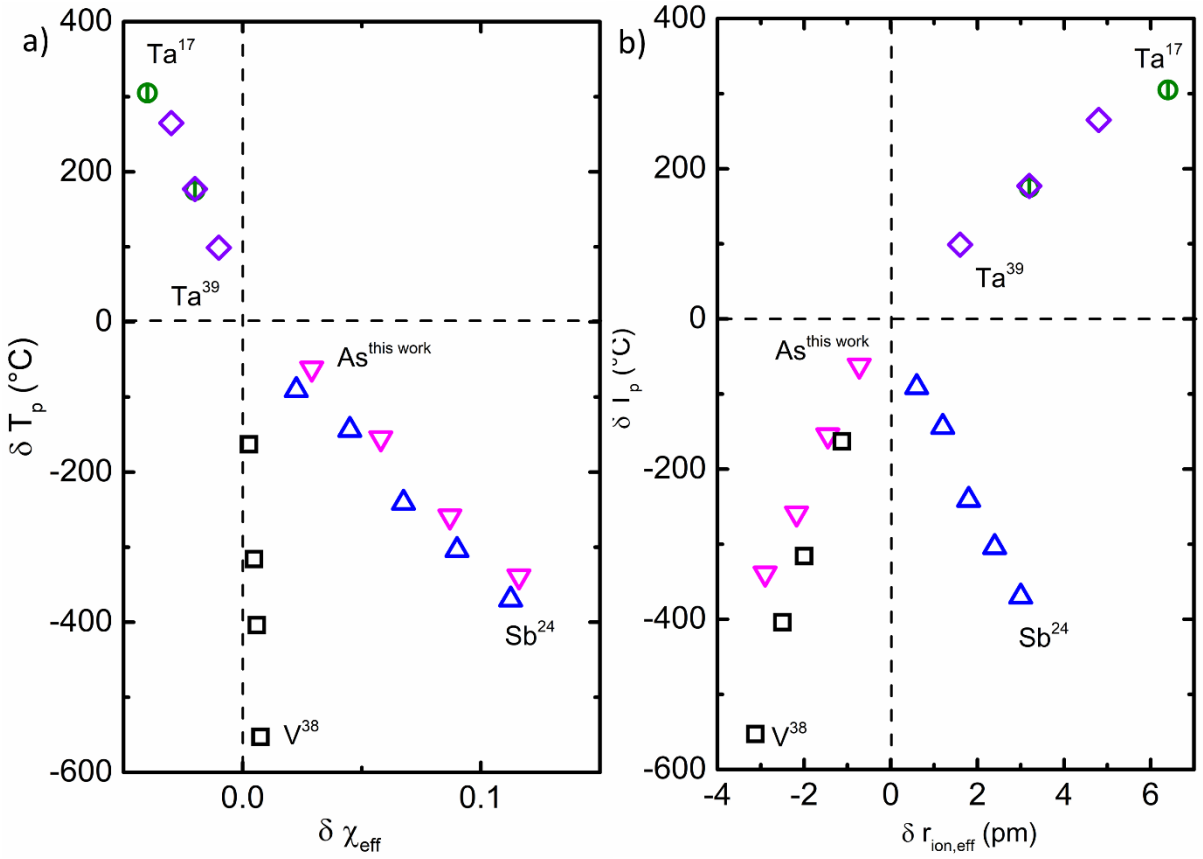

Figure 7. Deviation of the phase transition temperature in $LaNb_{1-x}M_xO_4$ (M = V, Ta, As or Sb) as a function of a) effective electronegativity and b) effective ionic radius of B-site ion.

Combining two factors together – electronegativity and ionic radius – we suggest that the former is a determining factor for the type of stabilization induced by the substituent, whereas the latter may be used as a predictor of how 'good' the stabilizer would be. Although, caution should be taken while predicting the effect of applying the substituent since the relation is a non-trivial interplay between those two factors.

5. Conclusions

In this work, the studies of the influence of As substitution on the structure and thermomechanical properties of lanthanum orthoniobates were performed. The structural properties were discussed in view of the available in the literature broad range of data on lanthanum orthoniobates with different isovalent substitutions.

It has been shown that single phase materials with general formula $LaNb_{1-x}As_xO_4$ ($0.5 \leq x \leq 0.30$) can be obtained with the combined co-precipitation and solid-state synthesis method.

It has been shown that As is stabilizing tetragonal polymorph of lanthanum orthoniobate. The phase transition temperature decreases linearly with increasing As content and it can be shifted

from 495 °C (undoped specimen) below room temperature (for 30 mol.% substituted sample). At room temperature $LaNb_{0.7}As_{0.3}O_4$ was tetragonal, $LaNb_{0.75}As_{0.25}O_4$ was a mixture of tetragonal and monoclinic phases, whilst all the other samples were monoclinic. In comparison to other substituents presented in the literature such as V, Ta or Sb, As is a better stabilizer of the tetragonal polymorph of lanthanum orthoniobate than Sb, but worse than V.

Thermal expansion coefficients – of both monoclinic and tetragonal polymorphs – are decreasing with increasing As content. This was explained by the increasing strength of the bonding between La^{3+} ions and BO_4^{3-} tetrahedra.

Comparative analysis of all substituents showed that both ionic radius and electronegativity of the substituent plays an important role for phase stabilization. The relation between the two factors is non-trivial, however, some general trends have been given. Thus, while electronegativity is a determining factor for the type of stabilization (monoclinic or tetragonal) induced by the substituent, the ionic radius may be used as a predictor of how 'good' the stabilizer would be.

Acknowledgements

This research work was financially supported by the National Science Centre, Poland Grant No. 2015/17/N/ST5/02813.

References

1 J. G. Kim, B. Son, S. Mukherjee, N. Schuppert, A. Bates, O. Kwon, M. J. Choi, H. Y. Chung and S. Park, *J. Power Sources*, 2015, **282**, 299–322.

2 T. Norby, *Solid State Ionics*, 1999, **125**, 1–11.

3 H. Iwahara, Y. Asakura, K. Katahira and M. Tanaka, *Solid State Ionics*, 2004, **168**, 299–310.

4 W. G. Coors, *J. Power Sources*, 2003, **118**, 150–156.

5 J. Molenda, J. Kupecki, R. Baron, M. Blesznowski, G. Brus, T. Brylewski, M. Bucko, J. Chmielowiec, K. Cwieka, M. Gazda, A. Gil, P. Jasinski, Z. Jaworski, J. Karczewski, M. Kawalec, R. Kluczowski, M. Krauz, F. Krok, B. Lukasik, M. Malys, A. Mazur, A. Mielewczyk-Gryn, J. Milewski, S. Molin, G. Mordarski, M. Mosialek, K. Motylinski, E. N. Naumovich, P. Nowak, G. Pasciak, P. Pianko-Oprych, D. Pomykalska, M. Rekas, A. Sciazko, K. Swierczek, J. Szmyd, S. Wachowski, T. Wejrzanowski, W. Wrobel, K. Zagorski, W. Zajac and A. Zurawska, *Int. J. Hydrogen Energy*, 2017, **42**, 4366–4403.

6 K. Zagórski, S. Wachowski, D. Szymczewska, A. Mielewczyk-Gryń, P. Jasiński and M. Gazda, *J. Power Sources*, 2017, **353**, 230–236.

7 N. Bausá, C. Solís, R. Strandbakke, J. M. Serra, S. J. M. Bausa Nuria, Solis Cecilia, Strandbakke Ragnar, N. Bausá, C. Solís, R. Strandbakke, J. M. Serra and S. J. M. Bausa Nuria, Solis Cecilia, Strandbakke Ragnar, *Solid State Ionics*, 2017, **306**, 62–68.

8 C. Kokkofitis, M. Ouzounidou, A. Skodra and M. Stoukides, *Solid State Ionics*, 2007, **178**, 507–513.

9 S. H. Morejudo, R. Zanón, S. Escolástico, I. Yuste-Tirados, H. Malerød-Fjeld, P. K. Vestre, W. G. Coors, A. Martínez, T. Norby, J. M. Serra and C. Kjølseth, *Science (80-.).*, 2016, **353**, 563–566.

10 H. Malerød-Fjeld, D. Clark, I. Yuste-Tirados, R. Zanón, D. Catalán-Martinez, D. Beeaff, S. H. Morejudo, P. K. Vestre, T. Norby, R. Haugsrud, J. M. Serra and C. Kjølseth, *Nat. Energy*, 2017, 1–9.

11 H. Iwahara, *Solid State Ionics*, 1992, **52**, 99–104.

12 R. Haugsrud and T. Norby, *Nat. Mater.*, 2006, **5**, 193–196.

13 P. Berger, F. Mauvy, J.-C. Grenier, N. Sata, A. Magrasó, R. Haugsrud and P. R. Slater, in *Proton-Conducting Ceramics: From Fundamentals to Applied Research*, ed. M. Marrony, Pan Stanford Publishing, Singapore, 2016, pp. 1–72.

14 T. Norby, M. Widerøe, R. Glöckner and Y. Larring, *Dalt. Trans.*, 2004, 3012–3018.

15 R. Haugsrud, *Diffus. Found.*, 2016, **8**, 31–79.

16 A. Magrasó, M.-L. Fontaine, R. Bredesen, R. Haugsrud and T. Norby, *Solid State Ionics*, 2014, **262**, 382–387.

17 F. Vullum, F. Nitsche, S. M. Selbach and T. Grande, *J. Solid State Chem.*, 2008, **181**, 2580–2585.

18 T. Mokkelbost, H. L. Lein, P. E. Vullum, R. Holmestad, T. Grande and M.-A. Einarsrud, *Ceram. Int.*, 2009, **35**, 2877–2883.

19 A. Mielewczyk-Gryn, S. Wachowski, K. Zagórski, P. Jasiński and M. Gazda, *Ceram. Int.*, 2015, **41**, 7847–7852.

20 A. D. Brandão, I. Antunes, J. R. Frade, J. Torre, V. V. Kharton and D. P. Fagg, *Chem. Mater.*, 2010, **22**, 6673–6683.

21 M. Ivanova, S. Ricote, W. A. Meulenberg, R. Haugsrud and M. Ziegner, *Solid State Ionics*, 2012, **213**, 45–52.

22 S. Wachowski, A. Mielewczyk-Gryń, K. Zagórski, C. Li, P. Jasiński, S. J. Skinner, R. Haugsrud and M. Gazda, *J. Mater. Chem. A*, 2016, **4**, 11696–11707.

23 Y. Cao, N. Duan, X. Wang, B. Chi, L. Jian, JianPu and L. Jian, *J. Eur. Ceram. Soc.*, 2015, **35**, 1979–1983.

24 S. Wachowski, A. Mielewczyk-Gryn and M. Gazda, *J. Solid State Chem.*, 2014, **219**, 201–209.

25 H. Fjeld, D. M. Kepaptsoglou, R. Haugsrud and T. Norby, *Solid State Ionics*, 2010, **181**, 104–109.

26 T. Mokkelbost, I. Kaus, R. Haugsrud, T. Norby, T. Grande and M.-A. Einarsrud, *J. Am. Ceram. Soc.*, 2008, **91**, 879–886.

27 A. B. Santibáñez-Mendieta, E. Fabbri, S. Licoccia and E. Traversa, *Solid State Ionics*, 2012, **216**, 6–10.

28 S. Tsunekawa, T. Kamiyama, K. Sasaki, H. Asano and T. Fukuda, *Acta Crystallogr. Sect. A Found. Crystallogr.*, 1993, **49**, 595–600.

29 W. I. F. David, *MRS Proc.*, 1989, **166**, 203.

30 V. S. Stubican, *J. Am. Ceram. Soc.*, 1964, **47**, 55–58.

31 M. Huse, A. W. B. Skilbred, M. Karlsson, S. G. Eriksson, T. Norby, R. Haugsrud and C. S. Knee, *J. Solid State Chem.*, 2012, **187**, 27–34.

32 L. Jian and C. M. Wayman, *Mater. Lett.*, 1996, **26**, 1–7.

33 H. Takei and S. Tsunekawa, *J. Cryst. Growth*, 1977, **38**, 55–60.

34 H. Fjeld, K. Toyoura, R. Haugsrud and T. Norby, *Phys. Chem. Chem. Phys.*, 2010, **12**, 10313–10319.

35 A. Mielewczyk-Gryn, S. Wachowski, K. I. Lilova, X. Guo, M. Gazda and A. Navrotsky, *Ceram. Int.*, 2015, **41**, 2128–2133.

36 Y. Cao, Y. Tan, D. Yan, B. Chi, J. Pu and L. Jian, *Solid State Ionics*, 2015, **278**, 152–156.

37 Y. Cao, B. Chi, J. Pu and L. Jian, *J. Eur. Ceram. Soc.*, 2014, **34**, 1981–1988.

38 A. T. Aldred, S.-K. Chan, M. H. Grimsditch and M. V. Nevitt, *MRS Proc.*, 1983, **24**, 81.

39 Z. Bi, C. A. Bridges, J.-H. Kim, A. Huq and M. P. Paranthaman, *J. Power Sources*, 2011, **196**, 7395–7403.

40 Y. Cao, N. Duan, X. Wang, B. Chi and L. Jian, *J. Eur. Ceram. Soc.*, 2015, **35**, 1979–1983.

41 T. S. Bjørheim, T. Norby and R. Haugsrud, *J. Mater. Chem.*, 2012, **22**, 1652.

42 R.-C. Juan, *Comm. powder Diffr. (IUCr). Newsl.*, 2001, **26**, 12–19.

43 M. Schmidt, U. Muller, R. Cardoso Gil, E. Milke and M. Binnewies, *Zeitschrift fur Anorg. und Allg. Chemie*, 2005, **631**, 1154–1162.

44 K. Momma and F. Izumi, *J. Appl. Crystallogr.*, 2011, **44**, 1272–1276.

45 K. Momma and F. Izumi, *J. Appl. Crystallogr.*, 2011, **44**, 1272–1276.

46 A. Mielewczyk-Gryn, K. Gdula-Kasica, B. Kusz and M. Gazda, *Ceram. Int.*, 2013, **39**,

4239–4244.

47 H. Li, S. Zhou and S. Zhang, *J. Solid State Chem.*, 2007, **180**, 589–595.

48 A. Mielewczyk-Gryn, S. Wachowski, J. Strychalska, K. Zagórski, T. Klimczuk, A. Navrotsky and M. Gazda, *Ceram. Int.*, 2016, **42**, 7054–7059.

49 R. D. Shannon and C. T. Prewitt, *Acta Crystallogr. Sect. B Struct. Crystallogr. Cryst. Chem.*, 1969, **25**, 925–946.

50 J. P. Bastide, *J. Solid State Chem.*, 1987, **71**, 115–120.

51 D. Errandonea and F. Manjon, *Prog. Mater. Sci.*, 2008, **53**, 711–773.

52 M. Nevitt and G. Knapp, *J. Phys. Chem. Solids*, 1986, **47**, 501–505.